JOURNAL OF COMPUTATIONAL PHYSICS 122, 68–82 (1995)

Effective Vorticity–Velocity Formulations for Three-Dimensional Incompressible Viscous Flows

X. H. WU, J. Z. WU, AND J. M. WU

The University of Tennessee Space Institute, Tullahoma, Tennessee 37388

Received October 11, 1994; revised March 10, 1995

The vorticity—velocity formulation for incompressible viscous flows is studied. The main concern is effective numerical solution of the kinematic Cauchy–Riemann equations for velocity, especially when the divergence-free condition of vorticity is violated due to numerical error. The mathematical formulation of a differential and an integral approaches are revisited. A novel projection of vorticity onto the divergence-free space and its application to the two approaches are studied. As an illustration of the differential approach, the 3D lid-driven cavity problem is solved. The projection scheme is justified through numerical tests by comparing it to a new fully divergence-free scheme. Numerical tests indicate that keeping vorticity divergence-free is important for obtaining correct and accurate solutions. The theory and methods apply to other divergence-free fields of physical interest as well, such as that in electro-magnetic dynamics.

I. INTRODUCTION

In many physical problems one needs to recover a vector field from its curl and divergence. Mathematically, this is known as solving the Cauchy–Riemann type of equations

$$\nabla \cdot \mathbf{u} = \vartheta, \quad \nabla \times \mathbf{u} = \boldsymbol{\omega} \quad \text{in } V, \qquad \text{(1a),(1b)}$$

for $\mathbf{u}$ from given ϑ and $\boldsymbol{\omega}$. Here V is a bounded domain in R^3. The physical meaning of (1a), (1b) can be found in classical electro-magnetic dynamics, but here we illustrate them in terms of fluid dynamics. Hence, $\mathbf{u}$, ϑ, and $\boldsymbol{\omega}$ are velocity, dilatation, and vorticity, respectively, which we assume to have desired smoothness on the closure of V. To uniquely determine $\mathbf{u}$, boundary conditions need to be prescribed. A common choice is

$$\mathbf{n} \cdot \mathbf{u} = u_n \quad \text{on } \partial V, \qquad \text{(1c)}$$

where ∂V and $\mathbf{n}$ are the boundary of V and its outward normal. The compatibility conditions

$$\int_V \vartheta \, dV = \oint_{\partial V} u_n \, dS, \quad \nabla \cdot \boldsymbol{\omega} = 0, \qquad \text{(2a),(2b)}$$

are necessary for (1) to have a solution. If (2) holds, Eq. (1) is well posed as proved in [1].

In numerical methods of computational fluid dynamics based on vorticity and dilatation, rather than primitive variables, solving (1) is a major kinematic step. Since (1) is elliptic, it is usually the most time-consuming part of the whole computation. Therefore, it is highly desirable to develop efficient methods, especially in unsteady computations, where (1) has to be solved in each time step.

Various approaches can be used to solve the above problem numerically. One is to discretize (1) directly by using the finite-difference method and to solve the resulting linear system of equations. Several fast solvers based on this approach have been proposed and studied for 2D problems [2–5]. However, these solvers are difficult to be extended to 3D, since the three equations in (1b) are not independent (this problem does not occur in 2D). Huang and Ghia [6] solve the problem by using a "ghost" variable, which contains roughly the scalar and vector potentials of $\mathbf{u}$, to reformulate the linear system of equations. A multigrid method is then developed to solve the reformulated system. The authors also pointed out that the Laplacian operator contained in the reformulated system gives a better smoothing rate for the relaxation than the original system. Another approach is based on a least square method proposed by Fix and Rose [1]. The method was used by Gatski *et al.* [7] to solve incompressible flow problems (see also [8]).

The main difficulty of the above direct approaches is that in 3D the vorticity $\boldsymbol{\omega}$, often obtained numerically, may have nonvanishing divergence due to numerical error. Thus, Eq. (1) does not have a solution and the direct method is no longer effective. The common remedy is to project $\boldsymbol{\omega}$ onto the divergence-free space before solving (1) as in [7]. The projection is defined by

$$\hat{\boldsymbol{\omega}} = \boldsymbol{\omega} - \nabla \psi, \quad \nabla \cdot \hat{\boldsymbol{\omega}} = 0, \qquad (3)$$

where $\hat{\boldsymbol{\omega}}$ is the projected vorticity. Thus ψ satisfies

$$\Delta \psi = \nabla \cdot \boldsymbol{\omega}. \qquad (4)$$

0021-9991/95 $12.00

One can obtain $\nabla\psi$ and, hence, $\hat{\boldsymbol{\omega}}$ by solving the Poisson equation (4). This approach, however, is time consuming. Furthermore, the above projection is not uniquely defined for bounded domain unless certain boundary condition of ψ is prescribed on ∂V, which needs to be properly selected based on some mathematical and physical criteria. One of the main objectives of this paper is thus to find proper projection and efficient methods.

Besides the direct solution, three alternative approaches have been employed. The first is to decompose $\mathbf{u}$ into scalar and vector potentials and solve the resulting equations for the potentials. Then, four Poisson equations need to be solved for a general 3D problem. In addition, the boundary condition of the vector potential may be difficult to specify; for a comprehensive discussion, see [9]. In short, the difficulty is present for multiply-connected domain, where the boundary conditions of the vector potential [9] involve the tangential components of $\mathbf{u}$ which are generally unknown in advance. It might be argued that for viscous flow problems, the no-slip condition can be used to specify those tangential components on solid boundaries. However, this usually leads to coupled solution of the vector potential and the vorticity field, which could be inefficient especially for unsteady problems. Note that Huang and Ghia's [6] approach is similar to this one but is technically different in that the ghost variable is never explicitly solved.

The present paper will mainly concern the other two approaches that do not introduce additional variables. One is based on the Poisson equation for $\mathbf{u}$ and the other, on the generalized Biot–Savart law. Both can be derived from the vector identity

$$\Delta\mathbf{u} = \nabla(\nabla\cdot\mathbf{u}) - \nabla\times(\nabla\times\mathbf{u}). \tag{5}$$

We call the former the *differential approach* and the latter the *integral approach*. Although these formulations are not new, some confusion and misunderstanding remain to be clarified. More importantly, we show that an optimum projection of $\boldsymbol{\omega}$ can be performed very efficiently when these two formulations are used.

The paper is organized as the following. In Sections 2, we define an optimum projection of vorticity and derive the corresponding boundary value problem. Then we revisit the differential and integral approaches for (1). In particular, we show how the optimum projection can be embedded in both approaches and efficiently computed. As an illustration, we use the vorticity–velocity formulation to solve the benchmark 3D lid-driven cavity flows, of which the numerical methods are given in Section 3. Only differential approach with projection is implemented, whereas the integral approach requires much more computing capacity and is not pursued here. A fully divergence-free scheme for the vorticity equation is also constructed and compared with the projection method. Numerical results are presented in Section 4. We make some concluding remarks in Section 5.

2. THEORY

2.1. *The Projection of Vorticity and Its Optimization*

We first present a rational basis of proper projections. As mentioned above, the problem we are facing is due to the numerical discretization of continuous equations. In a free space, the projection is uniquely defined and is orthogonal (in the L_2 sense) [10], assuming that $\boldsymbol{\omega}\to 0$ at infinity with proper rate. For bounded domain, the projection is determined by the boundary condition of ψ. An example, used in [7] without explanation, is

$$\frac{\partial\psi}{\partial n} = 0 \quad \text{on } \partial V. \tag{6}$$

Here, the key issue is to choose projections that preserves the numerical accuracy as well as the physical content of the solution. First, if the projected vorticity is closer to the unprojected one, then we have a better reason to believe that less useful information is lost during the projection. The projection will be called *optimum* if the projected vorticity is closest to the unprojected one. Secondly, the projection should have no effect on $\boldsymbol{\omega}$ when $\nabla\cdot\boldsymbol{\omega} = 0$; clearly, the projection defined by (4) and (6) satisfies this requirement.

Mathematically, we can formulate the first requirement as minimizing the difference between $\boldsymbol{\omega}$ and $\hat{\boldsymbol{\omega}}$ by imposing a proper boundary condition on ψ. In the L_2 norm we minimize

$$\mathbf{I}(\psi) = \int_V (\boldsymbol{\omega} - \hat{\boldsymbol{\omega}})^2\, dV = \int_V (\nabla\psi)^2\, dV.$$

Let ψ be the minimizing function and let $\psi + \varepsilon\psi'$ be a variation of ψ. Clearly ψ' must be harmonic in V, and hence it satisfies

$$\oint_{\partial V} \frac{\partial\psi'}{\partial n}\, dS = 0. \tag{7}$$

By the standard minimization argument, it is straightforward to show that

$$\int_V \nabla\psi\cdot\nabla\psi'\, dV = \oint_{\partial V} \psi\frac{\partial\psi'}{\partial n}\, dS = 0 \tag{8}$$

must be valid for all ψ'.

Now we show that

$$\psi = \text{const} \quad \text{on } \partial V \tag{9}$$

is the correct boundary condition. Obviously, if (9) is true, then (8) holds for all ψ', and ψ is a minimizing function. Conversely, if (9) is not true, it is always possible to construct ψ' such that (8) is violated. We give a proof of this assertion for 2D case. Assume ψ is not constant but a function of the arc length s of

∂V, then there exists an interval $[-s_0, s_0]$ on which $\psi(s)$ does not change sign and increases (or decreases) monotonically. Let ·

$$\frac{\partial \psi'}{\partial n} = \begin{cases} s(|s| - s_0)^2, & \text{if } s \in [-s_0, s_0], \\ 0, & \text{otherwise,} \end{cases}$$

which is a smooth function of s. Thus (7) holds and the corresponding harmonic function ψ' exists; however,

$$\oint_{\partial V} \psi \frac{\partial \psi'}{\partial n} ds = \int_{-s_0}^{s_0} \psi \frac{\partial \psi'}{\partial n} ds \neq 0.$$

For 3D problems, similar construction of ψ' can be done, but it is more complicated. We conclude that (9) is the *necessary and sufficient condition for the optimum projection*. Equivalent to (9) is the condition

$$\mathbf{n} \times \nabla \psi = 0 \quad \text{on } \partial V. \tag{10}$$

When $\nabla \cdot \boldsymbol{\omega} = 0$, the optimum projection does nothing. Moreover, the projection is orthogonal in the L_2 sense because

$$\int_V \hat{\boldsymbol{\omega}} \cdot \nabla \psi \, dV = \oint_{\partial V} \psi (\mathbf{n} \cdot \hat{\boldsymbol{\omega}}) \, dS = \psi \int_V \nabla \cdot \hat{\boldsymbol{\omega}} \, dV = 0.$$

From this equation, we see that the projection defined by (4) and (6) is also orthogonal if $\mathbf{n} \cdot \hat{\boldsymbol{\omega}} = \mathbf{n} \cdot \boldsymbol{\omega} = 0$, but *not* always.

Finally, it should be noted that the optimum projection defined above depends on what norm is used; also the solution of $\mathbf{u}$ depends on the projection of vorticity and hence the boundary condition of ψ. In general, it is difficult to judge the influence of different projections on the results. One may need to rely on numerical tests. In Section 4 we shall present some test results using the above optimum projection defined by the L_2 norm.

2.2. *The Differential Approach*

An effective way of solving problem (1) is substituting (1a), (1b) into (5), and then solving the Poisson equation for $\mathbf{u}$:

$$\Delta \mathbf{u} = \nabla \vartheta - \nabla \times \boldsymbol{\omega}. \tag{11a}$$

Since (11a) is one order higher than (1), more boundary conditions are needed in addition to (1c). These conditions have to exclude the spurious solutions from raising the order of the equations, so that a solution of (11a) is also that of (1). These conditions turn out to be the tangential part of (1b) (see discussion below). A very similar problem exists for the vorticity transport equation which is the curl of the Navier–Stokes equation, and the proper boundary condition for vorticity has also been found to be the tangential part of the Navier–Stokes equation [11]. Now the boundary conditions for (11a) are

$$\mathbf{n} \cdot \mathbf{u} = u_n, \quad \mathbf{n} \times (\nabla \times \mathbf{u} - \boldsymbol{\omega}) = 0 \quad \text{on } \partial V. \tag{11b),(11c}$$

This formulation has been used by [12] in their computation. However, the property of (11) has not been fully clarified. Here we prove the following.

THEOREM 2.1. *Suppose* (2a) *holds. Given sufficiently smooth* ϑ *and* $\boldsymbol{\omega}$, *problem* (11) *has a unique solution. Moreover, the solution satisfies the following equations (almost anywhere) in V,*

$$\nabla \cdot \mathbf{u} = \vartheta, \quad \nabla \times \mathbf{u} = \hat{\boldsymbol{\omega}}, \tag{12}$$

where $\hat{\boldsymbol{\omega}} = \boldsymbol{\omega} - \nabla \psi$ *and* ψ *is given by* (4) *and* (10).

Proof. We first show that the solution of (11) exists and is unique, then prove that it satisfies (12).

The existence of solution is a dirct consequence of (1) being well-posed. This is clear from the above derivation of (11) when $\nabla \cdot \boldsymbol{\omega} = 0$. If $\nabla \cdot \boldsymbol{\omega} \neq 0$, consider

$$\nabla \cdot \mathbf{u} = \vartheta, \quad \nabla \times \mathbf{u} = \hat{\boldsymbol{\omega}} \quad \text{in } V$$
$$\mathbf{n} \cdot \mathbf{u} = u_n \quad \text{on } \partial V,$$

where $\hat{\boldsymbol{\omega}} = \boldsymbol{\omega} - \nabla \psi$ and ψ satisfies (4) and (10). Since $\nabla \cdot \hat{\boldsymbol{\omega}} = 0$, the above set of equations is the same as (1) except that $\boldsymbol{\omega}$ is replaced by $\hat{\boldsymbol{\omega}}$; hence it has a unique solution. This solution satisfies (11a), as can be verified by using (5) and noticing that $\nabla \times \hat{\boldsymbol{\omega}} = \nabla \times \boldsymbol{\omega}$. The boundary condition (11c) is also satisfied due to (10).

Next, we show that (11) has at most one solution. Let $\mathbf{v}$ be the difference of two solutions of (11), such that

$$\Delta \mathbf{v} = 0, \quad \mathbf{n} \cdot \mathbf{v} = 0, \quad \mathbf{n} \times (\nabla \times \mathbf{v}) = 0.$$

Then, owing to the identity

$$\int_V [(\nabla \cdot \mathbf{v})^2 + (\nabla \times \mathbf{v})^2] \, dV$$
$$= -\int_V \mathbf{v} \cdot \Delta \mathbf{v} \, dV$$
$$+ \oint_{\partial V} [(\mathbf{n} \cdot \mathbf{v}) \nabla \cdot \mathbf{v} + (\nabla \times \mathbf{v}) \cdot (\mathbf{n} \times \mathbf{v})] \, dS,$$

and since

$$(\nabla \times \mathbf{v}) \cdot (\mathbf{n} \times \mathbf{v}) = -[\mathbf{n} \times (\nabla \times \mathbf{v})] \cdot \mathbf{v} = 0,$$

the right-hand side of the above integral equation vanishes. Thus, we have $\nabla \cdot \mathbf{v} = 0$ and $\nabla \times \mathbf{v} = 0$ (almost everywhere), implying $\mathbf{v} = \nabla \phi$ for some harmonic function ϕ. But

$\partial\phi/\partial n = 0$ on ∂V because of (1c); so $\phi =$ const. and hence $\mathbf{v} = 0$ in V.

Finally, from (11a) we have

$$\nabla(\nabla\cdot\mathbf{u} - \vartheta) - \nabla\times(\nabla\times\mathbf{u} - \boldsymbol{\omega}) = 0. \tag{14}$$

Since (11c) is sufficient for the two terms in (14) be orthogonal (in the L_2 sense), i.e.,

$$\int_V \nabla(\nabla\cdot\mathbf{u} - \vartheta)\cdot[\nabla\times(\nabla\times\mathbf{u} - \boldsymbol{\omega})]\,dV = \oint_{\partial V}[\mathbf{n}\times(\nabla\times\mathbf{u} - \boldsymbol{\omega})]\cdot\nabla(\nabla\cdot\mathbf{u} - \vartheta)\,dS = 0;$$

it follows that

$$\nabla(\nabla\cdot\mathbf{u} - \vartheta) = 0, \quad \nabla\times(\nabla\times\mathbf{u} - \boldsymbol{\omega}) = 0. \tag{15a),(15b}$$

Thus $\nabla\times\mathbf{u} - \boldsymbol{\omega} = -\nabla\psi$ for some scalar function ψ. Taking divergence of both sides we obtain (4); furthermore, (11c) implies Eq. (10). Similarly, we have $\nabla\cdot\mathbf{u} - \vartheta =$ const. in V, but the constant must be zero due to (2a). ▌

Remarks. 1. The significance of the theorem is that $\mathbf{u}$ can be solved from (11) with *arbitrary* $\boldsymbol{\omega}$, which may not be divergence-free. Moreover, the solution always has the correct divergence and its curl is nothing but the optimum projection of $\boldsymbol{\omega}$ (see Section 2.1). Thus, numerically, the projection can be performed simply by *differentiation* at little cost, instead of the time-consuming inversion of a Poisson equation.

2. The above remark also indicates that, whenever possible, we may solve only one or two components of $\mathbf{u}$ in 2D or 3D, respectively, and then compute the other by integrating (1a). Numerically, this gives roughly 50% and 33% saving of the CPU time in 2D and 3D. If projection is needed, the saving in 3D could be as much as 50%.

From Theorem 2.1 and its proof, the following corollary is obvious.

COROLLARY 2.1. *If* (2a),(2b) *holds, then given sufficiently smooth* ϑ *and* $\boldsymbol{\omega}$, (11) *and* (1) *have the same solution.*

The boundary condition (11c) deserves a more detailed discussion, because it is of crucial importance for obtaining the above results. Other boundary conditions were derived in [12]; however, in our opinion, only (11c) is the correct choice as far as solving (1) alone is considered. To see this, we first recall the least square argument of [13]. Consider minimizing the functional

$$\mathbf{J}(\mathbf{u}) = \int_V [(\nabla\cdot\mathbf{u} - \vartheta)^2 + (\nabla\times\mathbf{u} - \boldsymbol{\omega})^2]\,dV,$$

under the constraint of (1c). It can be shown that

$$-\int_V \mathbf{v}\cdot(\Delta\mathbf{u} - \nabla\vartheta - \nabla\times\boldsymbol{\omega})\,dV + \int_{\partial V}[(\nabla\cdot\mathbf{u} - \vartheta)(\mathbf{n}\cdot\mathbf{v}) + (\nabla\times\mathbf{u} - \boldsymbol{\omega})\cdot(\mathbf{n}\times\mathbf{v})]\,dS \tag{16}$$

must vanish for any admissible function $\mathbf{v}$ satisfying $\mathbf{n}\cdot\mathbf{v} = 0$. As a consequence, Eq. (11a) follows.

To assure the boundary integral of (16) is zero, we need to impose boundary conditions for $\mathbf{u}$. In [13], it was concluded that $\nabla\times\mathbf{u} - \boldsymbol{\omega} = 0$ should be specified on ∂V in addition to (1c). But, writing the last integrand in the boundary integral of (16) as $[(\nabla\times\mathbf{u} - \boldsymbol{\omega})\times\mathbf{n}]\cdot\mathbf{v}$, we see that (11c) is already sufficient.

Two other alternatives were derived from (16) in [12]:

$$\mathbf{u} = \mathbf{b} \quad \text{on } \partial V, \tag{17a}$$

$$\mathbf{n}\times\mathbf{u} = \mathbf{n}\times\mathbf{b}, \quad \nabla\cdot\mathbf{u} = \vartheta \quad \text{on } \partial V, \tag{17b}$$

However, both of them are incorrect. The solution of (11a) with (17a) may not satisfy the original Cauchy–Riemann equation (1) even if $\nabla\cdot\boldsymbol{\omega} = 0$. In fact, Eq. (17a) makes (1) overdetermined; i.e., the solution exists for only a restricted class of $\boldsymbol{\omega}$ due to the constraint on tangential components of $\mathbf{u}$ on ∂V. If a viscous flow is to be computed, the use of (17a) is acceptable only if (11) is coupled with the vorticity transport equation so that the proper $\boldsymbol{\omega}$ distribution can be ensured. The objection to (17b) is that it does not secure (1c) (total mass conservation for incompressible flows).

2.3. *The Integral Approach*

The integral approach based on the Biot–Savart law has also been frequently adopted, as in vortex methods. It has some advantages over the differential formulation; for example, the allowance of a grid-free algorithm that naturally matches the Lagrangian convection and of the exact treatment of the far field condition. However, some important details in implementing the integral approach have been widely ignored when the domain is bounded. In particular, when $\mathbf{n}\cdot\boldsymbol{\omega} \neq 0$ on ∂V, the commonly used method fails (see below). Besides, in vortex methods the integrals are often discretized with smoothed kernels instead of singular ones to gain more accuracy and better stability. This leads to the so-called vortex-blob discretization, which usually does not satisfy the divergence-free condition of vorticity and, hence, projection is again needed. However, how to perform such projection efficiently when the domain is bounded has never been addressed.

Let $G = G(\mathbf{x}, \mathbf{y})$ be the fundamental solution of the Laplace equation in free space, such that $\Delta G = -\delta(\mathbf{x} - \mathbf{y})$, and let

$\mathbf{g} = \nabla_y G(\mathbf{x}, \mathbf{y})$ (where ∇_y is the gradient operator with respect to $\mathbf{y}$). By (5) and the identity

$$\nabla\cdot(G\nabla\mathbf{u} - \mathbf{u}\nabla G) - \nabla(G\nabla\cdot\mathbf{u}) + \nabla\times(G\nabla\times\mathbf{u}) = -\nabla\cdot(\mathbf{u}\nabla G) + \nabla(\nabla G\cdot\mathbf{u}) - \nabla\cdot(\nabla G\mathbf{u}),$$

the generalized Biot–Savart law follows from Green's second identity:

$$\alpha\mathbf{u} = \int_V (\mathbf{g}\vartheta - \mathbf{g}\times\boldsymbol{\omega})\,dV - \oint_{\partial V}[\mathbf{g}(\mathbf{n}\cdot\mathbf{u}) - \mathbf{g}\times(\mathbf{n}\times\mathbf{u})]\,dS. \tag{18}$$

Here the integration is taken with respect to $\mathbf{y}$, and $\alpha = 1, 0,$ or $\frac{1}{2}$ for $\mathbf{x}$ in V, $V' = R^3\backslash\overline{V}$, or on a smooth ∂V, respectively. If an exterior domain is under consideration, we need to assume that as $|\mathbf{x}| \to \infty$, ϑ, and $\boldsymbol{\omega}$ are of order $|\mathbf{x}|^{-2}$ and $\mathbf{u} = 0$. Note that in (18) we have substituted (1a),(1b) in place of $\nabla\cdot\mathbf{u}$ and $\nabla\times\mathbf{u}$, respectively, which implies that (2a),(2b) are satisfied. However, it is important to remember that in actual computations Eq. (2b) may be violated because of numerical error.

Since the generalized Biot–Savart law is derived from (5), whether it is equivalent to the original equation (1) needs to be verified. A detailed proof is given in [14]. In this paper, we are interested in the computation procedure of $\mathbf{u}$. One way is to use (1c) and (18) to obtain a boundary integral equation (BIE) of $\mathbf{n}\times\mathbf{u}$; see [15]. Here, we follow the approach of Lighthill [16], which is more often used and easier to implement.

Denote the volume integral in (18) as $\mathbf{u}_v$, then $\mathbf{u}$ may be expressed as

$$\mathbf{u} = \mathbf{u}_v + \mathbf{u}_s. \tag{19}$$

In general, $\mathbf{u}_v$ alone does not satisfy (1c); thus we need to find $\mathbf{u}_s$ (i.e., the surface integral in (18)) such that $\mathbf{u}$ satisfies (1c). It has been commonly argued that $\mathbf{u}_s$ is irrotational "since $\nabla\times\mathbf{u}_v = \boldsymbol{\omega}$" (Refs. [16, 17]) and, hence, $\mathbf{u}_s = \nabla\phi$. Then because $\nabla\cdot\mathbf{u}_v = 0$ and, hence, $\nabla\cdot(\mathbf{u} - \mathbf{u}_v) = 0$, there is

$$\Delta\phi = 0, \tag{20a}$$

$$\frac{\partial\phi}{\partial n} = u_n - \mathbf{n}\cdot\mathbf{u}_v. \tag{20b}$$

Equation (20) can be solved uniquely and the desired $\mathbf{u}$ is obtained.

Unfortunately, when $\mathbf{n}\cdot\boldsymbol{\omega} \neq 0$ on ∂V, which may occur in 3D, the above argument fails because $\nabla\times\mathbf{u}_v \neq \boldsymbol{\omega}$. Instead, we have

$$\nabla\times\mathbf{u}_v = -\int_V \nabla_x\times(\mathbf{g}\times\boldsymbol{\omega})\,dV = \boldsymbol{\omega} - \int_V(\nabla\cdot\boldsymbol{\omega})\mathbf{g}\,dV + \oint_{\partial V}(\mathbf{n}\cdot\boldsymbol{\omega})\mathbf{g}\,dS \tag{21}$$
$$= \boldsymbol{\omega} + \oint_{\partial V}(\mathbf{n}\cdot\boldsymbol{\omega})\mathbf{g}\,dS \quad (\text{if } \nabla\cdot\boldsymbol{\omega} = 0).$$

Nevertheless, the above method can be modified to cover general 3D problems. Following [18], we define the extension of vorticity $\boldsymbol{\omega}' = \nabla\phi'$ in V' (similarly for exterior problems), where ϕ' satisfies

$$\Delta\phi' = 0 \quad \text{in } V', \tag{22a}$$

$$\frac{\partial\phi'}{\partial n} = \mathbf{n}\cdot\boldsymbol{\omega} \quad \text{on } \partial V, \tag{22b}$$

$$\nabla\phi' \to 0 \quad \text{as } |\mathbf{x}| \to \infty. \tag{22c}$$

Then, let

$$\mathbf{u} = \mathbf{u}_v + \mathbf{u}_s' + \mathbf{u}_s'', \tag{23}$$

where

$$\mathbf{u}_s' = -\int_{V'}\mathbf{g}\times\nabla\phi'\,dV = -\oint_{\partial V}\phi'(\mathbf{n}\times\mathbf{g})\,dS. \tag{24}$$

It is easy to verify that

$$\nabla\cdot\mathbf{u}_s' = 0, \quad \nabla\times\mathbf{u}_s' = \beta\nabla\phi' - \oint_{\partial V}(\mathbf{n}\cdot\boldsymbol{\omega})\mathbf{g}\,dS,$$

where $\beta = 0$ or 1 for $\mathbf{x}$ in V or V', respectively. Thus,

$$\nabla\times\mathbf{u}_s'' = \nabla\times\mathbf{u} - \nabla\times(\mathbf{u}_v + \mathbf{u}_s') = 0 \quad \text{in } V.$$

Therefore, $\mathbf{u}_s'' = \nabla\phi''$ is uniquely defined, with ϕ'' given by

$$\Delta\phi'' = 0 \quad \text{in } V, \tag{25a}$$

$$\frac{\partial\phi''}{\partial n} = u_n - \mathbf{n}\cdot(\mathbf{u}_v + \mathbf{u}_s') \quad \text{on } \partial V. \tag{25b}$$

Then, the solution of (1) is obtainable from (23).

Using the above procedure, we can compute the tangential components of $\mathbf{u}$ on ∂V by solving and evaluating quantities solely on the boundary. Essentially, this is equivalent to solving the BIE for $\mathbf{n}\times\mathbf{u}$ mentioned above. This is obvious if we note that once $\mathbf{u}_v$ on ∂V is evaluated, we can compute $\mathbf{u}_s'$ and $\mathbf{u}_s''$ from boundary values of ϕ' and ϕ'', which in turn can be solved from BIEs corresponding to (22) and (25). We also note that in the above integral method, only $\mathbf{u}_v$ needs to be evaluated by a volume integral. Both volume and surface integrals as well as BIEs for ϕ' and ϕ'' can be computed/solved efficiently by

using the fast multipole method (FMM) [19–21]. An efficient scheme based on FMM has been used to solve the boundary-integral equations of potential problems with arbitrary geometry [19, 22]. These advances make the above scheme ready to implement numerically.

Consider now the above procedure with $\nabla \cdot \boldsymbol{\omega} \neq 0$. In free space, the velocity computed from the Biot–Savart law automatically corresponds to the projected vorticity as shown in [10], which is similar to the differential approach in the previous subsection. For bounded domain, in general, the above procedure cannot be used without modification. Since $\nabla \cdot \boldsymbol{\omega} \neq 0$,

$$\oint_{\partial V} \mathbf{n} \cdot \boldsymbol{\omega}\, dS \neq 0$$

might occur; hence the harmonic function ϕ' defined by (22) might not exist. In the following, we give a modified version *with the optimum projection built in.*

Our goal is to obtain $\mathbf{u}$ such that $\nabla \times \mathbf{u} = \hat{\boldsymbol{\omega}}$, where $\hat{\boldsymbol{\omega}}$ is given by (3) and (10). First, we observe that the general projection of $\boldsymbol{\omega}$ can be formulated in integral form as

$$\begin{aligned} \hat{\boldsymbol{\omega}} = \boldsymbol{\omega} - \int_V \mathbf{g}(\nabla \cdot \boldsymbol{\omega})\, dV + \oint_{\partial V} \mathbf{n} \cdot (\boldsymbol{\omega} - \hat{\boldsymbol{\omega}})\mathbf{g}\, dS \\ + \oint_{\partial V} \mathbf{g} \times (\mathbf{n} \times (\boldsymbol{\omega} - \hat{\boldsymbol{\omega}}))\, dS. \end{aligned} \tag{26}$$

For the optimum projection, the last integral on the right-hand side of (26) is zero. It is easy to see that if we replace $\mathbf{n} \cdot \boldsymbol{\omega}$ in (22b) by $\mathbf{n} \cdot \hat{\boldsymbol{\omega}}$, then ϕ' exits and $\nabla \times (\mathbf{u}_v + \mathbf{u}_s') = \hat{\boldsymbol{\omega}}$. Then $\nabla \times \mathbf{u}_s'' = 0$ and the rest of the construction remains the same. From (21) and (26), we get a BIE for $\mathbf{n} \cdot \hat{\boldsymbol{\omega}}$

$$\mathbf{n} \cdot \hat{\boldsymbol{\omega}} = (\mathbf{n} \times \nabla) \cdot \mathbf{u}_v - \mathbf{n} \cdot \oint_{\partial V} \mathbf{g}(\mathbf{n} \cdot \hat{\boldsymbol{\omega}})\, dS, \tag{27}$$

where the last integral should be understood as the limit as the control point $\mathbf{x} \to \partial V$. Note that the first term on the right-hand side of (27) indicates that only $\mathbf{u}_v$ on ∂V is needed. Moreover, when $\nabla \times \mathbf{u} = \boldsymbol{\omega}$ (i.e., $\nabla \cdot \boldsymbol{\omega} = 0$), Eq. (27) can be recast to a homogeneous BIE of $\mathbf{n} \cdot (\boldsymbol{\omega} - \hat{\boldsymbol{\omega}})$, which can be shown to allow only a trivial solution (Ref. [14]); then $\boldsymbol{\omega} = \hat{\boldsymbol{\omega}}$ follows.

In summary, when $\nabla \cdot \boldsymbol{\omega} \neq 0$, only one more BIE needs to be solved to build the optimum projection into the resulting $\mathbf{u}$ solution. Compare with solving the projection in the whole domain, this is much more efficient. The key of efficiency is to fully utilize the information contained in $\mathbf{u}_v$ due to the volume integral.

3. NUMERICAL METHODS

In this section, we develop vorticity-velocity methods for solving 3D incompressible flows using finite-difference method based on previous theoretical results. Only the differential approach is addressed. The integral approach demands much more computing power and, hence, is not pursued further below. We use Cartesian coordinate for demonstration. The scheme can be easily extended to generalized orthogonal coordinates if the covariance variables of [23] are used; in this case, the component-wise formulation has exactly the same form as in Cartesian coordinates.

The main objective of the present numerical study is to verify that our projection method indeed works correctly. Such a numerical test is necessary, since the effect of projection is hard to analyze mathematically. Furthermore, it is commonly believed that the divergence-free condition of vorticity is important, but there is no serious numerical experiment to show the influence of the error in the divergence of vorticity. Again, this information is hard to obtain from the usual consistency and stability analyses. As we show later, the computation is stable even with large error in the divergence of vorticity, but the result could be wrong. In the meantime, the results show that our projection is an efficient way to ensure the correct results. For this purpose, we choose the standard lid-driven cavity flow as the test problem (Fig. 1). Although it is simple, the flow exhibits complex 3D vortical structures, especially at high Reynolds number. Therefore, the flow may be sensitive to the error in vorticity.

For more realistic flows, one may need to specify the in-flow, out-flow, and free-stream conditions. For a review of computations of such flow problems using vorticity–velocity methods, see Gatski [8]. Although applying our optimum projection method to improve the computation of these flows is beyond the scope of the present paper, it seems appropriate to include a brief discussion of these conditions in the context of the present formulation. For the velocity $\mathbf{u}$, the problem is universal among all numerical methods for incompressible flows, and a great deal of research has been done. There are no new requirements raised by the present formulation. But we stress that the discrete analog of (2a), which includes in-flow, out-flow boundaries, etc., should be satisfied to ensure $\nabla \cdot \mathbf{u} = 0$ at discrete levels. For the vorticity $\boldsymbol{\omega}$, however, the present projection formulation gives rise to some desirable flexibility. Note that (2a) should also hold for $\boldsymbol{\omega}$ due to $\nabla \cdot \boldsymbol{\omega} = 0$. But, for the present formulation, this requirement need *not* be imposed explicitly; unlike velocity, it is already automatically taken care of by the optimum projection. In contrast, if the projection given by (6) is used, special care is still necessary since the projection preserves $\mathbf{n} \cdot \boldsymbol{\omega}$ on ∂V.

3.1. *The Kinematic Equations*

At the first sight, it might seem to be straightforward to discretize (11) and solve the resulting linear system of equations. But a usual discretization of (11) might *not* behave as predicted by the theory, since the vector identities used in theoretical derivations may be violated during discretizations. A basic observation is that, due to the truncation error, the

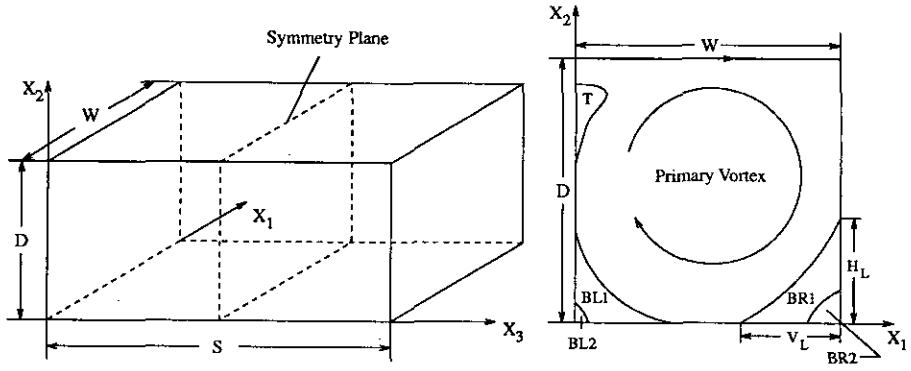

FIG. 1. The lid-driven cavity flow. Left: Three-dimensional configuration. Right: Vortex structures of two-dimensional flow; T, BL, and BR stand for top, bottom-left, and bottom-right vortices, respectively.

mixed derivatives with different order may not cancel each other exactly in their discrete forms. Numerical schemes are often more predictable and stable if they preserve the properties of their continuous counterparts. Thus, we prefer the discrete cancellation to be precise at the round-off level. A simple way to achieve this is to define the discrete differential operators (difference operators) in each direction uniquely and to maintain the functions uniquely defined on the grid [14]. The second requirement is often met automatically, but in certain cases it needs special attention (see Section 3.2 below).

A uniform staggered grid as depicted in Fig. 2 is used to discretize (11). This grid has proved to be valuable for preserving mass conservation [23, 24], i.e., (1a). For the present problem it has two more advantages: it is easy to impose boundary condition (11c), and it is convenient to perform the numerical projection of $\boldsymbol{\omega}$ on the staggered grid.

In the following, we assume $\vartheta = 0$ as our numerical example is an incompressible flow. Let i, j, and k denote the grid indices along x_α ($\alpha = 1, 2, 3$) directions; wherever necessary for clarity, we raise the index of vector components to a superscript. According to Fig. 2, the velocity components are defined as $u^1_{i,j+1/2,k+1/2}$, $u^2_{i+1/2,j,k+1/2}$, and $u^3_{i+1/2,j+1/2,k}$; and the vorticity components are $\omega^1_{i+1/2,j,k}$, $\omega^2_{i,j+1/2,k}$, and $\omega^3_{i,j,k+1/2}$. Define the discrete gradient operator as

$$\nabla^h = (D_1, D_2, D_3) = \left(\frac{\delta_1}{\Delta x_1}, \frac{\delta_2}{\Delta x_2}, \frac{\delta_3}{\Delta x_3}\right), \tag{28}$$

where δ_α and Δx_α are the central difference operator and grid size in the α-direction, respectively; hence $D_1 f_{i,j,k} = (f_{i+1/2,j,k} - f_{i-1/2,j,k})/\Delta x_1$, etc. We shall use the notation $(D_1 f)_{i,j,k} = D_1 f_{i,j,k}$ to group several operations together. Thus, the velocity and vorticity are related by

$$\omega^1_{i+1/2,j,k} = (D_2 u^3 - D_3 u^2)_{i+1/2,j,k},$$
$$\omega^2_{i,j+1/2,k} = (D_3 u^1 - D_1 u^3)_{i,j+1/2,k},$$
$$\omega^3_{i,j,k+1/2} = (D_1 u^2 - D_2 u^1)_{i,j,k+1/2},$$

which is in fact our projection scheme. It is easily verified

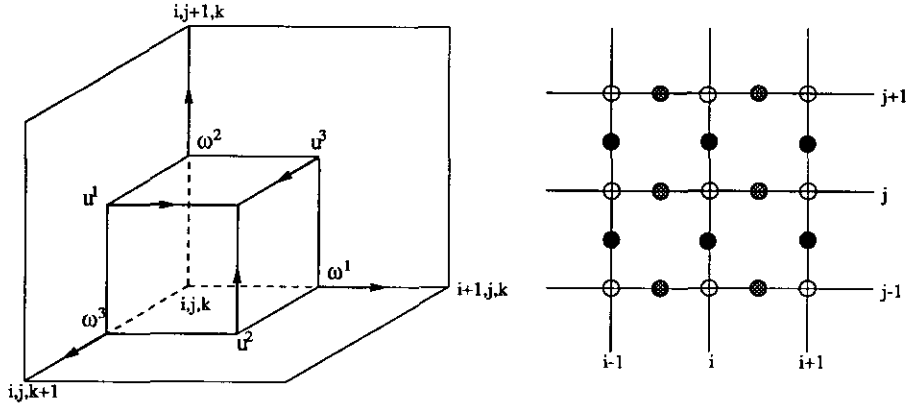

FIG. 2. The staggered grid for $\boldsymbol{\omega}$-$\mathbf{u}$ method. Left: The 3D grid. Right: The 2D grid; u^1, u^2 and ω^3 are defined on the black, gray, and white dots, respectively.

that the projected vorticity is divergence-free inside the domain, i.e.,

$$(D_1\omega^1 + D_2\omega^2 + D_3\omega^3)_{i,j,k} = 0.$$

The divergence of vorticity on the boundary has to be discretized differently in another way. We shall return to this issue in the next subsection when discussing the divergence-free schemes for 3D vorticity equation.

Using the above definition, the discretization of (11a) in x_1 direction is

$$(D^2u^1 = D_3\omega^2 - D_2\omega^3)_{i,j+1/2,k+1/2}, \tag{29a}$$

where $D^2 = (D_1^2 + D_2^2 + D_3^2) = \Delta^h$ is the discrete Laplacian operator. At the boundary we have

$$u^1_{i,j+1/2,k+1/2} = 0, \quad i = 1 \text{ and } N_1; \tag{29b}$$

$$D_2u^1_{i,j,k+1/2} = -\omega^3_{i,j,k+1/2}, \quad j = 1 \text{ and } N_2; \tag{29c}$$

$$D_3u^1_{i,j+1/2,k} = \omega^2_{i,j+1/2,k}, \quad k = 1 \text{ and } N_3. \tag{29d}$$

Here N_α is the number of grid points in α-direction. The scheme given by (29) is second order. By (29d) there is

$$D_3^2u^1_{i,j+1/2,k+1/2} = \frac{1}{\Delta x_3}(D_3u^1_{i,j+1/2,k+1} - D_3u^1_{i,j+1/2,k})$$

$$= \frac{1}{\Delta x_3}(D_3u^1_{i,j+1/2,k+1} - \omega^2_{i,j+1/2,k}) \quad (k = 1).$$

Note that $\omega^2_{i,j+1/2,1}$, a tangential vorticity component on the boundary, cancels the corresponding term in $D_3\omega^2_{i,j+1/2,1}$ on the right-hand side of (29a) and thereby does not appear in the linear system of equations. Similarly, neither does the boundary value of ω^3. Thus, Eq. (29) leads to a closed linear system of equations for interior values of u^1 without using tangential components of $\boldsymbol{\omega}$ on ∂V. Similar discretization can be done for u^2 and u^3. On the present uniform grid, Eq. (29) can be solved efficiently by using the fast Fourier transform. For nonuniform grids, other solution techniques, such as multigrid methods, can be used.

We shall show that the solution of $\mathbf{u}$ is indeed divergence-free in the sense that

$$\theta_{i+1/2,j+1/2,k+1/2} = (D_1u^1 + D_2u^2 + D_3u^3)_{i+1/2,j+1/2,k+1/2} = 0, \tag{30}$$

where $\theta = \nabla \cdot \mathbf{u}$, is identically satisfied. Note that θ should not be confused with ϑ; the former may or may not equal the latter, depending on the discretization of (11). Now, we need to solve only two components of $\mathbf{u}$, say u^1 and u^2, and compute u^3 from (30). To avoid the accumulation of round-off error at one end of the integration, we can alternate the direction of integration between time steps or stages in a multistage time-integration method.

We outline the proof that the above implementation does ensure (30). Although a proof of $\nabla \cdot \mathbf{u} = 0$ has been given in Section 2.2, it does not relate directly to the above discretization. But we may look at the continuous problem from another point of view, whose discrete analog provides a general way of proving (30) immediately: taking divergence of (11a) (with $\vartheta = 0$) yields

$$\Delta\theta = 0 \quad \text{in } V. \tag{31}$$

Moreover, from the proof of Theorem 2.1, we know that

$$\frac{\partial\theta}{\partial n} = 0 \quad \text{on } \partial V. \tag{32}$$

Thus $\theta = $ const. in V and, due to the compatibility condition (2a), there is $\theta = 0$ in V. Therefore, if we can show that the discrete analog of (31) and (32) holds, then the similar conclusion can be drawn for the discrete problem. Such an approach is rather independent of the grid, although only a uniform Cartesian grid is considered here. For higher-order methods, the same principle applies. By (29) and the corresponding equations for u^2 and u^3, it is straightforward to verify

$$D^2\theta_{i+1/2,j+1/2,k+1/2} = 0 \tag{33}$$

for $i = 2, \ldots, N_1 - 2$; $j = 2, \ldots, N_2 - 2$; $k = 2, \ldots, N_3 - 2$. For the rest of the grid points in the neighborhood of the cavity walls, edges, and corners, special derivation needs to be made. At the first glance, if we can derive (33) on these near-boundary points and show that the discrete version of (32),

$$D_1\theta_{i,j+1/2,k+1/2} = 0 \quad \text{for } i = 1 \text{ and } N_1 - 1 \tag{34a}$$

$$D_2\theta_{i+1/2,j,k+1/2} = 0 \quad \text{for } j = 1 \text{ and } N_2 - 1 \tag{34b}$$

$$D_3\theta_{i+1/2,j+1/2,k} = 0 \quad \text{for } k = 1 \text{ and } N_3 - 1, \tag{34c}$$

is valid on the boundary, then it is easy to find that the linear system of equations for θ has at most nontrivial constant solution, and the constant has to be zero because the summation of θ over the whole domain, i.e., the net mass flux out of the boundary, is zero.

However, it is impossible to derive (33) and (34) separately. Rather, when solving θ numerically, Eq. (34) is used to cancel the unknown boundary terms in (33), resulting in an equation of θ at grid points next to the boundary. Thus, it is indeed the combination of (33) and (34) that is important. Therefore, we only need to derive the equations for θ at next-to-boundary points and to show that they are the same as the above combina-

tion. We shall not go through the algebraic details here; interested readers are referred to [14].

We stress again that not every discretization of (11) can preserve the desired properties of the continuous problem; it is always desirable to check the numerical methods mathematically. The above procedure is a simple and general way to do so.

Finally, if $\vartheta \neq 0$, it should be given at the same location as θ, and (29a) should be revised by adding $D_1\vartheta$ to its right-hand side. With some minor changes, the proof outlined above can be used to show that $\theta = \vartheta$ is valid in the sense similar to (30). Note that the discrete distribution of ϑ needs to satisfy the compatibility condition (2a) in a way consistent with (29).

3.2. *The Vorticity Transport Equation*

We present a second-order scheme for solving unsteady vorticity transport equation. Then we combine it with the scheme for (11) to solve the 3D lid-driven cavity flow (Fig. 1) in the next section. The discretization is done on a uniform Cartesian grid. The extension to generalized coordinates is straightforward, e.g., [23].

The 3D vorticity transport equation can be written in divergence form

$$\frac{\partial \boldsymbol{\omega}}{\partial t} + \nabla \cdot (\mathbf{u}\boldsymbol{\omega} - \boldsymbol{\omega}\mathbf{u}) = \nu \Delta \boldsymbol{\omega} \quad \text{in } V, \tag{35}$$

where V is the interior of the cavity. A second-order Runge–Kutta scheme is used for the discretization in time. We only consider the spatial discretization in some detail.

The main problem of discretizing (35) is how to ensure $\boldsymbol{\omega}$ being divergence-free. Consider the semi-discretized version of (35)

$$\frac{\partial \boldsymbol{\omega}}{\partial t} + \nabla^h \cdot (\mathbf{u}\boldsymbol{\omega} - \boldsymbol{\omega}\mathbf{u}) = \nu \Delta^h \boldsymbol{\omega}, \tag{36}$$

of which the (discrete) divergence is

$$\frac{\partial \vartheta_\omega}{\partial t} = -\nabla^h \cdot [\nabla^h \cdot (\mathbf{u}\boldsymbol{\omega} - \boldsymbol{\omega}\mathbf{u})] + \nu \Delta^h \vartheta_\omega \quad \text{in } V, \tag{37}$$

where $\vartheta_\omega = \nabla^h \cdot \boldsymbol{\omega}$. Thus, to ensure $\vartheta_\omega = 0$, we need to guarantee that $\vartheta_\omega = 0$ initially and on ∂V; moreover, the first term on the right-hand side of (37) needs to be zero. In fact, all these conditions are met in the continuous problem. However, the last two conditions often do not hold for the discrete problem due to spatial truncation error as discussed in Section 3.1. Note that (37) is a diffusion equation with a source term. Therefore, although the truncation error is usually small, it may accumulate during the time marching to give a large error in ϑ_ω. For the same reason, the round-off error may also accumulate; but this is a less severe problem because it is normally much smaller than the truncation error and more or less random.

There are two methods to resolve the problem. One is the projection of vorticity as discussed in Sections 2.1 and 3.1; the other is using a fully divergence-free scheme, i.e., discretizing the vorticity equation in a careful manner so that the solution is divergence-free to the round-off level. The latter will be used to justify our projection method numerically. Some divergence-free schemes have been studied in [23, 24]. Both of them are based on central difference. Here we present a general way of constructing the spatial discretization that leads to divergence-free schemes. We expand (36) as

$$\left[\frac{\partial}{\partial t}\omega^1 + D_2(F^{21} - F^{12}) + D_3(F^{31} - F^{13}) = \nu D^2 \omega^1\right]_{i+1/2,j,k},$$

$$\left[\frac{\partial}{\partial t}\omega^2 + D_1(F^{12} - F^{21}) + D_3(F^{32} - F^{23}) = \nu D^2 \omega^2\right]_{i,j+1/2,k},$$

$$\left[\frac{\partial}{\partial t}\omega^3 + D_1(F^{13} - F^{31}) + D_2(F^{23} - F^{32}) = \nu D^2 \omega^3\right]_{i,j,k+1/2},$$

where

$$F^{\alpha\beta} = u^\alpha \omega^\beta, \quad \alpha, \beta = 1, 2, 3, \alpha \neq \beta.$$

From these equations, the equation for ϑ_ω can be derived as

$$\left\{\frac{\partial}{\partial t}\vartheta_\omega + \sum_{\alpha \neq \beta} [D_\alpha D_\beta (F^{\beta\alpha} - F^{\alpha\beta}) + D_\beta D_\alpha (F^{\alpha\beta} - F^{\beta\alpha})] = \nu D^2 \vartheta_\omega\right\}_{i,j,k}. \tag{38}$$

Thus, a divergence-free scheme requires

$$D_\alpha D_\beta (F^{\beta\alpha} - F^{\alpha\beta}) + D_\beta D_\alpha (F^{\alpha\beta} - F^{\beta\alpha}) = 0, \tag{39}$$

which might seem to be trivial from (38). However, one should keep in mind that $F^{\beta\alpha}$ represents the *convective* effect in the first term of (39) but vortex *stretching* effect in the second. In both cases the value of, say, $F^{21}_{i+1/2,j+1/2,k}$ (with different signs) is used. Since neither u^2 nor ω^1 is defined at $\{i + 1/2, j + 1/2, k\}$, interpolation is necessary. Then how to do it so that $F^{21}_{i+1/2,j+1/2,k}$ is *uniquely defined* and, hence, the desired cancellation in (38) will occur? An obvious answer is to *calculate $F^{21}_{i+1/2,j+1/2,k}$ only once, and use the result in both convection and stretching terms.*

Thus, we just need to consider the construction of $F^{21}_{i+1/2,j+1/2,k}$ as a convection term. First we interpolate $u^2_{i+1/2,j,k}$ from $u^2_{i+1/2,j,k+1/2}$. In the computation done below, we take

$$u^2_{i+1/2,j,k} = 0.5(u^2_{i+1/2,j,k+1/2} + u^2_{i+1/2,j,k-1/2}). \tag{40}$$

Thus, $F^{21}_{i+1/2,j,k} = (u^2\omega^1)_{i+1/2,j,k}$ can be evaluated. Next, we may interpolate $F^{21}_{i+1/2,j+1/2,k}$ (values at the cell interfaces) from $F^{21}_{i+1/2,j,k}$ by using various methods, such as QUICK and ENO type upwind schemes. Calculation of other flux values is done in the same way. If centered interpolation is used, the algorithm is similar to those in [23, 24]. It should be noted that defining $F^{\beta\alpha}$ uniquely is *sufficient* for the cancellation, but not necessary. However, the above method is the simplest and easiest to be extended to generalized coordinates and higher order.

To obtain a fully divergence-free scheme for vorticity, we still need to ensure that no error is produced from the boundary. We impose $\boldsymbol{\omega} = \nabla \times \mathbf{u}$ on ∂V. It follows that $\nabla \cdot \boldsymbol{\omega} = 0$ on the boundary and, hence, the divergence-free condition is ensured theoretically. Again, this argument does not guarantee numerical methods to have the same property.

As an example, we consider the vorticity boundary condition at the bottom of the cavity. In component form, they are

$$\omega^1 = \frac{\partial u^3}{\partial x^2}, \quad \omega^2 = 0, \quad \omega^3 = -\frac{\partial u^1}{\partial x_2}.$$

To get ω^1 and ω^3, local Taylor expansion of the velocity components is used. We have

$$u^3_{i+1/2,j+1/2,k} = u^3_{i+1/2,j,k} + \frac{\Delta x_2}{2}\omega^1_{i+1/2,j,k} + \frac{\Delta x_2^2}{8}\left(\frac{\partial^2 u^3}{\partial x_2^2}\right)_{i+1/2,j,k} + O(\Delta x_2^3),$$

$$u^1_{i,j+1/2,k+1/2} = u^1_{i,j,k+1/2} - \frac{\Delta x_2}{2}\omega^3_{i,j,k+1/2} + \frac{\Delta x_2^2}{8}\left(\frac{\partial^2 u^1}{\partial x_2^2}\right)_{i,j,k+1/2} + O(\Delta x_2^3)$$

for $j = 1$. If the second- and higher-order terms are ignored, applying the no-slip condition $u^3_{i+1/2,j,k} = u^1_{i,j+1/2,k} = 0$ gives first-order formulas for ω^1 and ω^3 at the boundary. Second-order formulas can be obtained by combining the above two expansions with those of $u^3_{i+1/2,j+3/2,k}$ and $u^1_{i,j+3/2,k+1/2}$. All these formulas can be written in the form of

$$\omega^1_{i+1/2,j,k} = I_2(u^3)/\Delta x_2, \quad \omega^3_{i,j,k+1/2} = -I_2(u^1)/\Delta x_2, \tag{41}$$

where $I_2(f)$ denotes a linear interpolation of f in x_2 direction. Note that the stencil information is contained in I_2.

While it is straightforward to apply the tangential kinematic BCs of vorticity, the normal vorticity condition needs to be treated more carefully. The normal condition $\omega^2_{i,1,k} = 0$ is not directly applicable because of the staggered grid. In fact $\omega^2_{i,1/2,k}$ is needed by the central difference for updating $\omega^2_{i,3/2,k}$ at a new time level. Thus extrapolation seems necessary. On the other hand, it can be shown that $\vartheta_{\omega,i,j,k}$ should vanish identically on ∂V so that no error of ϑ_ω enters the solution from the boundary. Therefore, there must be a consistency requirement on the extrapolation. In particular, at the bottom of the cavity, we require $\vartheta_\omega = 0$, i.e.,

$$D_2\omega^2_{i,j,k} = -D_1\omega^1_{i,j,k} - D_3\omega^3_{i,j,k} \quad (\text{for } j = 1).$$

Suppose the *same* interpolation operator is used for *both* tangential velocity components u^1 and u^3, then by (41) we have

$$\begin{aligned} D_2\omega^2_{i,j,k} &= -(\omega^1_{i+1/2,j,k} - \omega^1_{i-1/2,j,k})/\Delta x_1 - (\omega^3_{i,j,k+1/2} - \omega^3_{i,j,k-1/2})/\Delta x_3 \\ &= (-I_2(D_1u^3) + I_2(D_3u^1))/\Delta x_2 \\ &= I_2(\omega^2)/\Delta x_2. \end{aligned} \tag{42}$$

Thus, the extrapolation we are seeking is

$$\omega^2_{i,1/2,k} = \omega^2_{i,3/2,k} - I_2(\omega^2). \tag{43}$$

However, $D_2\omega^2$ is precisely just the discrete normal derivative of ω^2 at the boundary, which can be used directly in the computation. Therefore, the extrapolation is actually *not* performed. Furthermore, from (41) we can verify that (42) is consistent with

$$\omega^2_{i,1,k} = (D_3u^1 - D_1u^3)_{i,1,k} = 0,$$

which is the original normal condition we tried to use.

4. RESULTS

Now we present the results of the 3D lid-driven cavity. The flow was solved for both Re = 1000 and 3200 using the $\boldsymbol{\omega}$-$\mathbf{u}$ method described above. For Re = 1000, steady-state solution exists; whereas for Re = 3200, the flow is unsteady and has rather complicated 3D vortical structures. To reduce the computation, we imposed a spanwise symmetry condition at the symmetry plane (see Fig. 1) so that only half-cavity flow was actually solved. Such an approach is justifiable for Re = 3200 flow, although some Taylor–Görtler-like (TGL) vortices were moving around in the spanwise direction. Perng and Street [25] pointed out that the end walls provide only symmetric perturbations to the vortices, as confirmed by their numerical simulation of the full cavity flow.

The flow in a cavity with depth-to-width ration 1 : 1 and the span-to-width ratio 3 : 1 was investigated experimentally by Koseff and Street [26]. Later, numerical simulation at Re = 3200 was performed by Freitas *et al.* [27], using primitive variables, and by Tromeur-Dervout and Ta Phouc [28], Huang *et al.* [29], Huang and Ghia [6] (Re = 3300), using the $\boldsymbol{\omega}$-$\mathbf{u}$ method. Unfortunately, the accuracy of these simulations was not carefully verified. But for flows in a cubic cavity ($1 \times 1 \times 1$) at Re = 400 and 1000, accurate steady-state solutions were obtained by Ku *et al.* [30] using pseudospectral method. The problem was also solved recently by Guj and Stella [24]

using the ω-**u** method. Their results are in good agreement. Therefore, we shall use the solutions of [30] for checking the accuracy of our method. Then, a more interesting flow at Re = 3200 was simulated by different schemes. All results below (for the cubic cavity) are obtained on a 65 × 65 × 33 grid with single precision.

The projection type of method has been successfully used in several applications [8]. However, it has never been truly justified from a theoretical or numerical point of view. One of the main objectives of the following numerical tests was to see how well the projection method works comparing to fully divergence-free schemes. The comparison was done for both steady and unsteady flows. Another problem we investigated is the effect of different discretizations of the convection and stretching terms. Moreover, we made close observation of the effect of error in ϑ_ω on the solution.

Several schemes can be constructed by combining different discretizations of the convection and stretching terms, the vorticity BCs, and the projection. Thus, it is convenient to use short-handed names for the schemes. The following convention is used: a scheme labeled as A-B, say, means that the interpolation methods A and B are used for the convection and stretching terms (notice the order), respectively. Moreover, we shall use Q for QUICK and C for centered schemes. If the projection is used, then the label becomes A-B-P. Thus, Q-C-P means that the QUICK and centered interpolations are used for the convection and stretching, respectively, and projection is also used. From the previous discussion, we know that the Q-C scheme is not divergence-free; the Q-Q and C-C schemes are divergence-free but may not be fully divergence-free if error is introduced from the boundary.

In the present single-precision computation, we found that the accumulation of round-off error of ϑ_ω was rather severe. When steady-state solution is reached at about $t = 40$, the fully divergence-free Q-Q scheme gave ϑ_ω an averaged value of 5.83×10^{-4} and maximum value of 1.18×10^{-2}. A test using double precision was conducted and we found that ϑ_ω did not exceed 10^{-11} for the Q-Q scheme; thus the accumulation of round-off error has no effect on the solution.

The flow field in the cavity was projected onto x_1-x_2, x_2-x_3, and x_1-x_3 mid-planes and plotted in Fig. 3. They are in good agreement with Guj and Stella's results [24]. In the next two figures, the profile of u^1 on the vertical centerline and the profile of u^2 on the horizontal centerline of the symmetry plane are compared with the pseudospectral results of Ku *et al.* [30].

Figure 4 shows the results using first-order vorticity BC. It can be seen that all the solutions are in good agreement, except that the two schemes without projection are slightly less accurate, which is evidently due to larger error in ϑ_ω. The figure implies that even a seemingly small residual ϑ_ω (below 10^{-3} for the Q-Q scheme) might not be good enough. On the other hand, the averaged value of ϑ_ω at steady state due to the Q-C scheme is very large, (about 0.87); but interestingly, the flow field seems to be not severely affected by this error. We may

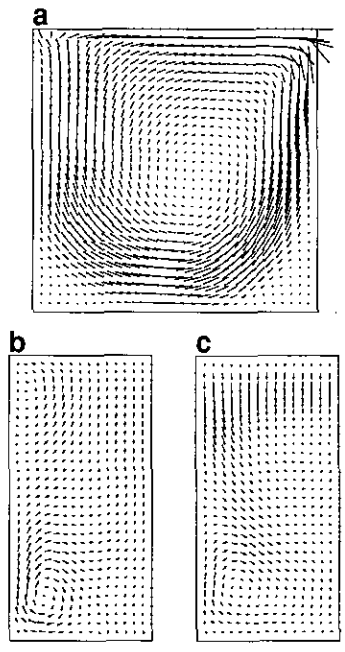

FIG. 3. Velocity vector plots for Re = 1000 flow projected on: (a) x_1-x_2 mid-plane; (b) x_2-x_3 mid-plane; (c) x_1-x_3 mid-plane.

explain this situation by noting that the divergence of vorticity corresponds to the second-order derivative of velocity; hence a small error in velocity field can be greatly amplified. Inversely, a large ϑ_ω does not necessarily mean a large error in **u**. In Table I, we present the differences among velocity fields solved from those schemes shown in Fig. 4. The table also shows that although the residual ϑ_ω of the Q-Q scheme is much smaller than that of the Q-C scheme, the difference between the velocity solutions of the Q-Q and Q-Q-P schemes is about the same as that between Q-C and Q-C-P schemes. Furthermore, the table indicates that the discretization of the stretching term does not have a strong influence on the present steady-state result, at least less than that due to ϑ_ω.

The second-order vorticity BC was also used with different schemes to solve the problem. In one scheme, labeled as Q-Q-PI (I for "inconsistent"), we intentionally used the second-order BC in a way violating the consistency requirement given in Section 3.2, so that in each time step a rather larger error of ϑ_ω was introduced on the boundary. Then, projection is used to filter the error out. Figure 5 compares the results of using first- (Q-Q-P1) and second-order BCs (Q-Q-P2 and Q-Q-PI). Clearly, the second-order BC leads to better accuracy. But, interestingly, the Q-Q-PI scheme seems to give the most accurate result, particularly the solution of u^2. Moreover, by comparing the **u** solutions of Q-Q-P, Q-C-P, and C-C-P, we find that the difference between Q-Q-P (or Q-C-P) and (C-C-P) (10^{-3}) is much larger than that between Q-Q-P and Q-C-P (10^{-4}). Therefore, the discretization of the convection term has a stronger effect on the results than that of the stretching term. In all cases, the projection worked very well.

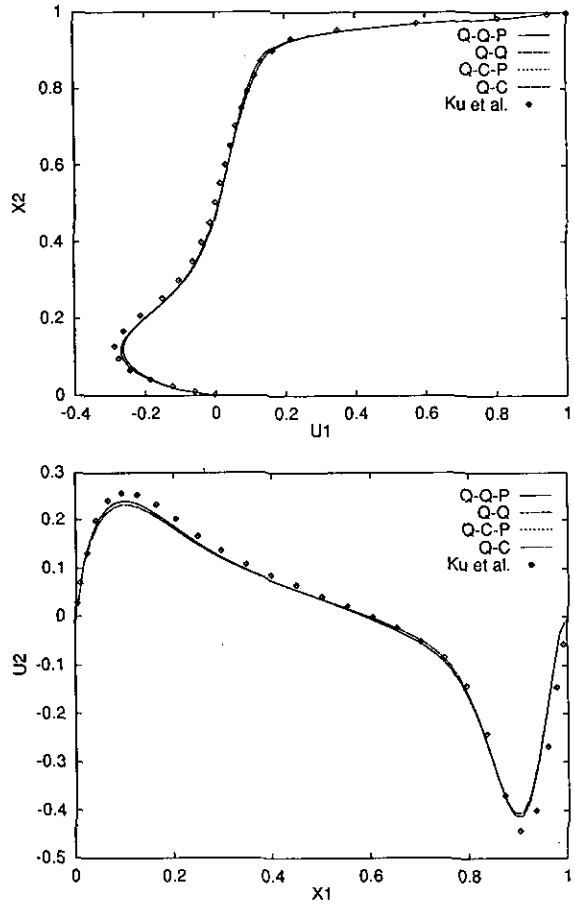

FIG. 4. Velocity profiles on centerlines of the symmetry plane using first-order vorticity BC. Top: u^1 profile; bottom: u^2 profile.

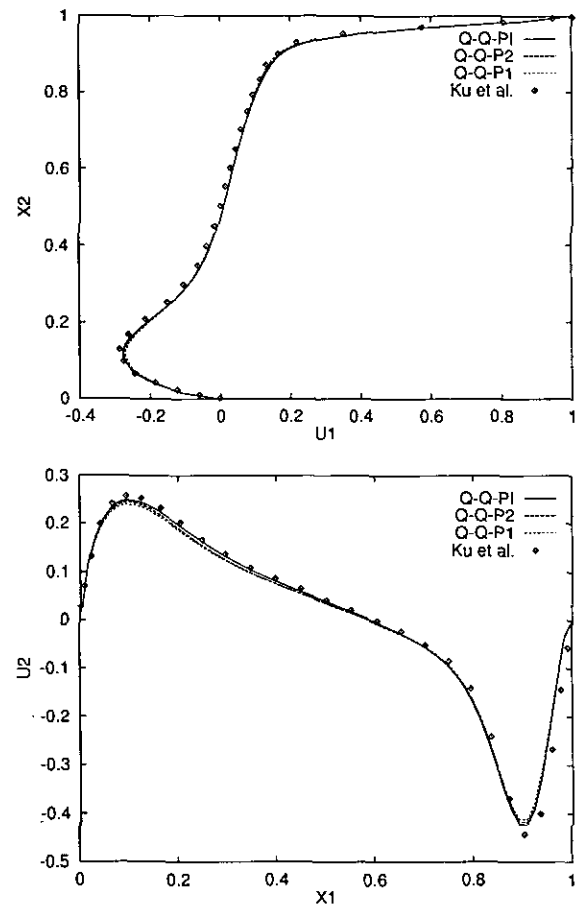

FIG. 5. Velocity profiles on centerlines of the symmetry plane (Re = 1000). Top: u^1 profile; bottom: u^2 profile.

At Re = 3200, the flow is unsteady and quite complicated. First, the primary vortex, as well as the upstream and downstream secondary vortices (see Fig. 1), developed. Then, the corner vortex and TGL vortices (see Fig. 7 below) started to form close to the downstream sidewall. The flow remained unsteady because of the meandering of TGL vortices and the variation in size of downstream secondary vortex. It was found experimentally that the TGL vortices are very time-dependent; thus a time-accurate numerical method is required to capture the flow features correctly. Unfortunately, due to the lack of accurate time-dependent experimental or numerical data, we cannot assess the actual time accuracy of our (formally second-order) methods. Since the corner vortex, which is due to the adjustment of shear and pressure forces acting on the recirculating fluid to the no-slip condition, has a strong influence on TGL vortices, we may also expect a strong effect of vorticity BCs and near-wall grid resolution on the numerical results.

TABLE I

L_2 Norm of Difference in Velocity Solved by Different Schemes

	Q-Q vs. Q-Q-P	Q-Q-P vs. Q-C-P	Q-C-P vs. Q-C	Q-C vs. Q-Q
u^1	3.32e-3	1.39e-4	3.56e-3	9.32e-4
u^2	3.30e-3	1.46e-4	3.62e-3	9.31e-4
u^3	2.60e-3	9.06e-6	7.98e-4	6.77e-4

According to [31], the flow reaches fully developed state about 6 min after the startup. In terms of our nondimensional time it is about $t = 51.2$. The projected velocity field on the symmetry plane at this time is shown in Fig. 6. Results of different schemes with the first-order vorticity BC are compared. Clearly, the result of the Q-C scheme is significantly different from others. The same can be seen from the comparison in Fig. 7, where **u** is projected onto $x_1 = 0.766$ plane (i.e., $i = 50$). The difference is caused by the large error in ϑ_ω (whose average is about 3.1) of the Q-C scheme. For the Q-Q scheme, the error accumulated from round-off seems to be independent of Re. The residual ϑ_ω at $t = 51.2$ is about the same as the Re = 1000 case. However, the speed of accumulation is slower. In contrast, for the Q-C scheme the residual ϑ_ω increases with Re because the diffusion of ϑ_ω out of the boundary is

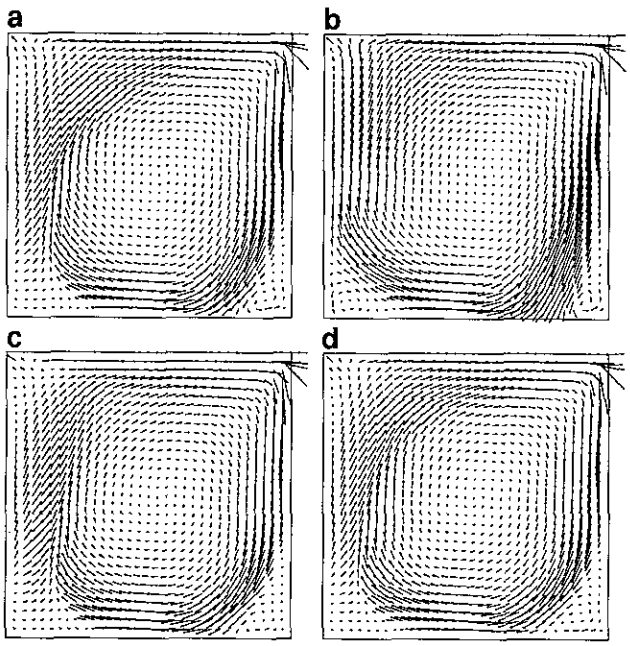

FIG. 6. Velocity field for Re = 3200 flow, projected in the symmetry plane: (a) Q-Q; (b) Q-C; (c) C-C-P; (d) Q-C-P.

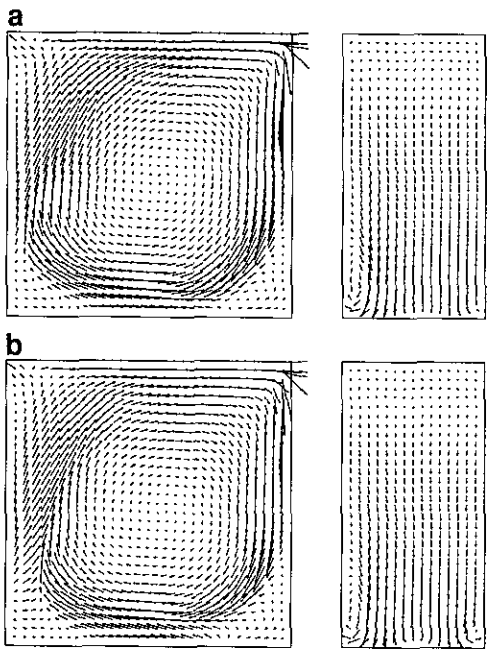

FIG. 8. Velocity field for Re = 3200 using second-order vorticity BC, projected in the symmetry plane (left) and x_1 = 0.766 plane (right): (a) Q-Q-P; (b) C-C-P.

weaker. It is plausible to conclude that for high-Re flows, the nondivergence-free scheme without projection is not appropriate.

In addition to the above observation, we note that there are some notable differences among the results of Q-C-P, C-C-P, and Q-Q, especially in Fig. 7. The only difference in these schemes is the discretization. Without a benchmark solution, we cannot judge which discretization is better here. The next figure, Fig. 8, shows the results of Q-Q-P and C-C-P schemes with second-order vorticity BC. Comparing Fig. 8 with Figs. 6 and 7, it may be concluded that the solution is more sensitive to the boundary condition than to the discretization of the vorticity equation.

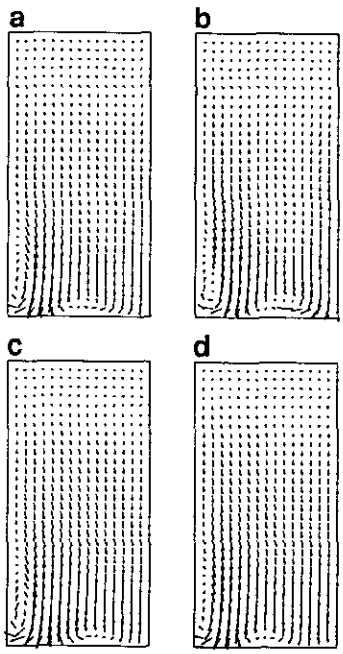

FIG. 7. Velocity field for Re = 3200, projected in x_1 = 0.766 plane: (a) Q-Q; (b) Q-C; (c) C-C-P; (d) Q-C-P.

Because our grid is rather coarse, especially at the boundary, the solutions we obtained here are only of qualitative value. Quantitative discussion of the time variation of the flow, particularly those features associated with the TGL vorticies, would not be informative. In Fig. 9, the time-averaged velocity profiles at the symmetry plane is compared with the experimental measurements [31]. The Q-Q-P scheme with first- and second-order BCs was used. Our time averages were obtained over the period of 7–10, 10–13, and 11–13 min after the startup. The experimental data are averages over a 5-min time period for the fully developed flow. The agreement is good considering the coarse grid. Perng and Street [25] used a nonuniform grid with grid size equals to 0.005 (ours is 0.0156) near the boundaries and we get excellent agreement by using a time average over the period of 7–10 min. However, it should be noted that the time average is affected by the time period used, at least in our computation (see Fig. 9). At last, Fig. 10 shows the velocity field computed using the Q-Q scheme with first-order BC at 7, 10, and 13 min after the startup. The figure shows possible structures of TGL vorticies, whose motion is complicated. Flow structures similar to Figs. 10a and 10b have also been reported

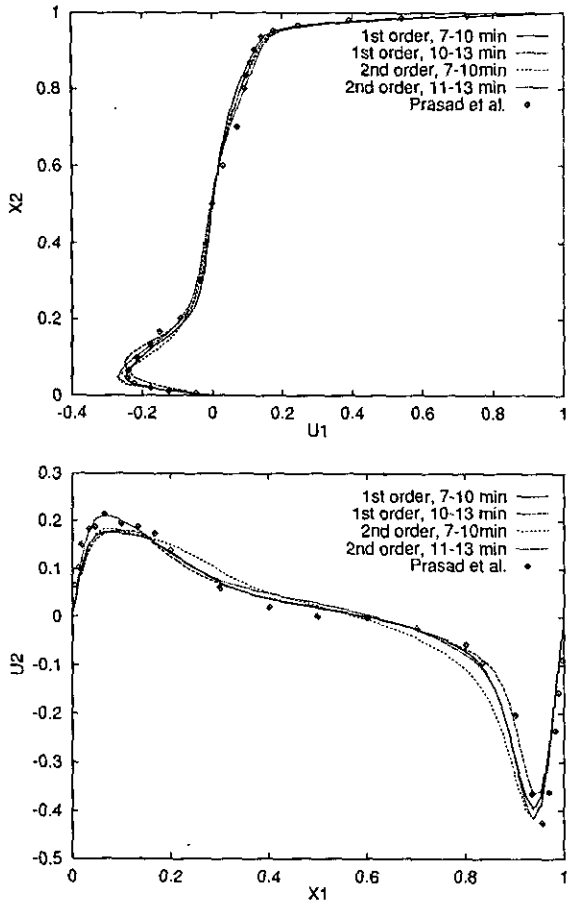

FIG. 9. Time averaged velocity profile at the symmetry plane (Re = 3200). Top: u^1 profile; bottom: u^2 profile.

in [25]. The current simulation seems to be able to capture fine vortex structures.

5. CONCLUDING REMARKS

The efficient vorticity–velocity formulation for 3D incompressible flows is studied both theoretically and numerically. Both differential and integral formulations are considered. We paid special attention to the problem of the divergence-free condition and the numerical methods to ensure it, including projection method and divergence-free schemes for the vorticity equation. An optimum projection formulation is proposed and tested through numerical experiments. The main feature of our formulation is that the solution of the velocity and the projection of the vorticity can be done in one step by solving (11).

Numerical tests show that the projection indeed gives accurate and correct results. In contrast, the divergence-free scheme constructed by special design of discretization is less flexible to use. This limitation may be more severe when extending the present scheme to higher order and more general geometry. In this case, the projection method is desirable in the sense that once we obtain the proper high-order scheme in general geometry for the kinematics part, which must be done anyway, we can construct high-order schemes for the vorticity equation with more freedom. However, the strategy used in constructing the divergence-free scheme in this paper is of general interest. In particular, in magneto-hydrodynamics, the magnetic field should be divergence-free; then the fully divergence-free method presented here can be used directly to discretize the magnetic field equation because it has exactly the same form as the vorticity equation. The optimum projection method can also be used. The same efficiency may be obtained if the right formulation like (11) can be found.

The effect of the divergence-free condition of vorticity is studied numerically for the first time. In conclusion, it is important to ensure the condition, using either the projection or the divergence-free scheme, to obtain correct physical results, especially at high Reynolds number. In the limit of inviscid flow, this condition could be of key importance. On the other hand, although our solution of the velocity field always has the

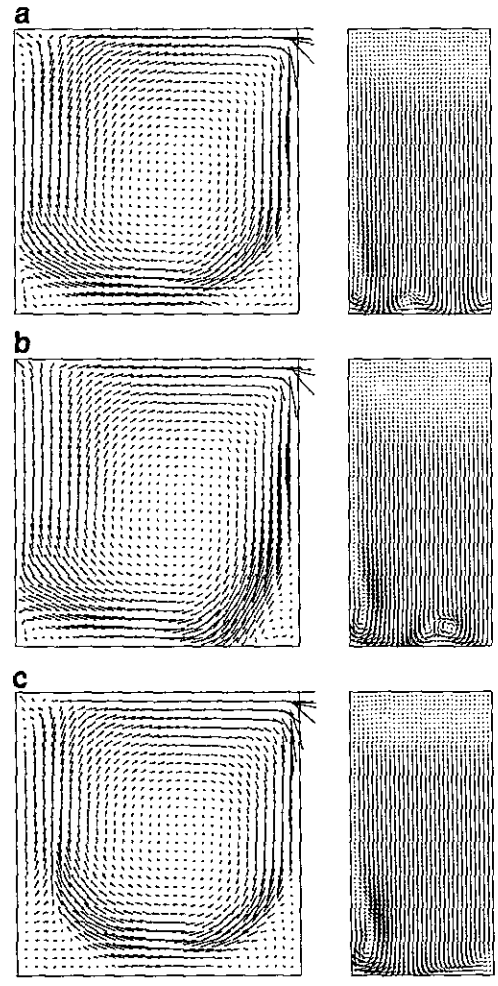

FIG. 10. Projected velocity field at symmetry plane (left) and $x_1 = 0.766$ plane (right) for Re = 3200 flow: (a) $t = 7$ min; (b) $t = 10$ min; (c) $t = 13$ min.

correct divergence, it alone does not guarantee the correct results.

REFERENCES

1. G. J. Fix and M. E. Rose, *SIAM J. Numer. Anal.* **22,** 250 (1985).
2. H. Martin, *J. Comput. Phys.* **15,** 55 (1974).
3. E. D. Martin and H. Lomax, Technical Report TN D-7934, NASA, 1977 (unpublished).
4. M. Balgovind, *Math. Comput.* **33,** 585 (1979).
5. R. E. Grosch, Technical Report 87-34, ICASE, 1987 (unpublished).
6. Y. Huang and U. Ghia, *Commun. Appl. Numer. Methods* **8,** 707 (1992).
7. T. B. Gatski, C. E. Grosch, and M. E. Rose, *J. Comput. Phys.* **82,** 298 (1989).
8. T. B. Gatski, *Appl. Numer. Math.* **7,** 227 (1991).
9. S. M. Richardson and A. R. H. Cornish, *J. Fluid Mech.* **82,** 309 (1977).
10. J. T. Beale, *Math. Comput.* **46,** 401 (1986).
11. J. Z. Wu, X. H. Wu, H. Y. Ma, and J. M. Wu, *Int. J. Numer. Methods Fluids* **19,** 905 (1994).
12. M. Hafez, J. Dacles, and M. Soliman, "A Velocity/Vorticity Method for Viscous Incompressible Flow Calculations," in *Proceedings, 11th International Conference on Numerical Methods in Fluid Dynamics, Williamsburg, VA, 1988,* p. 288.
13. T. N. Phillips, *IMA J. Numer. Anal.* **5,** 429 (1985).
14. X. H. Wu, Ph.D. thesis, University of Tennessee, Knoxville, 1994.
15. L. Morino, "Helmholtz and Poincaré Potential-Vorticity Decompositions for the Analysis of Unsteady Compressible Viscous Flows," in *Boundary Element Methods in Nonlinear Fluid Dynamics,* edited by P. K. Banerjee and L. Morino, Developments in Boundary Element Methods, Vol. 6 (Elsevier Appl. Sci., New York, 1990), p. 1.
16. M. J. Lighthill, in *Laminar Boundary Layers,* edited by L. Rosenhead (Oxford Univ. Press, Oxford, 1963).
17. E. Puckett, "Vortex Methods: An Introduction and Survey of Selected Research Topics," in *Incompressible Computational Fluid Dynamics,* edited by M. D. Gunzburger and R. A. Nicolaides (Cambridge Univ. Press, Cambridge, 1993).
18. J. Serrin, "Mathematical Principles of Classical Fluid Mechanics," in *Handbuch der Physik,* Volume VIII/1, edited by S. Flügge (Springer-Verlag, New York/Berlin, 1959), p. 125.
19. V. Rokhlin, *J. Comput. Phys.* **60,** 29 (1985).
20. L. Greengard and V. Rokhlin, *J. Comput. Phys.* **73,** 325 (1987).
21. J. Carrier, L. Greengard, and V. Rokhlin, *SIAM J. Sci. Stat. Comput.* **9,** 669 (1988).
22. A. Greenbaum, L. Greengard, and G. B. McFadden, *J. Comput. Phys.* **105,** 267 (1993).
23. G. A. Osswald, K. N. Ghia, and U. Ghia, AIAA Paper 87-1139, 1987 (unpublished).
24. G. Guj and F. Stella, *J. Comput. Phys.* **106,** 286 (1993).
25. C.-Y. Perng and R. L. Street, *Int. J. Numer. Methods Fluids* **9,** 341 (1989).
26. J. R. Koseff and R. L. Street, *J. Fluids Eng.* **106,** 390 (1984).
27. C. J. Freitas, R. L. Street, A. N. Findikakis, and J. R. Koseff, *Int. J. Numer. Methods Fluids* **5,** 561 (1985).
28. D. Tromeur-Dervout and L. T. Phuoc, Technical Report, ONERA TP 1991-235, 1991 (unpublished).
29. Y. Huang, U. Ghia, G. A. Osswald, and K. N. Ghia, AIAA Paper 91-1562, 1991 (unpublished).
30. H. C. Ku, R. S. Hirsh, and T. D. Taylor, *J. Comput. Phys.* **70,** 439 (1987).
31. A. K. Prasad, C. Y. Perng, and J. R. Koseff, "Some Observations of the Influence of Longitudinal Vorticies in a Lid-driven Cavity Flow," in *Proceedings, First Nat. Fluid Dynamics Congr., 1988,* p. 288.